Determining the phase of the structure factor by Kossel cone analysis with the use of synchrotron radiation

J. T. Hutton, G. T. Trammell, and J. P. Hannon
Physics Department, Rice University, Houston, Texas 77251
(Received 13 October 1983; revised manuscript received 4 June 1984)

We investigate the feasibility of using Bragg-case Kossel lines to measure phase angles of structure-factor amplitudes. Several experimental geometries utilizing a focused beam of synchrotron radiation to produce a suitable source are proposed. As an example, line profiles and excess integrated intensities are calculated for the [111] and [333] Ga Kossel lines from a GaAs crystal cut parallel to a (111) face. Sources of uncertainty and applicability of this technique are also discussed. The analysis shows that by using this method it should be possible to measure phase angles to within a few degrees, despite "smearing" of the line profiles due to angular resolution and the inherent linewidth of the emitted x rays.

I. INTRODUCTION

A central difficulty in determining charge distributions of crystals by x-ray analysis is the measurement of the phases of the structure factors. This problem is particularly acute in noncentrosymmetric crystals in which these phase angles may take on any value from 0 to 2π. Three major methods have been proposed to deal with this problem. The most widely used is the controlled variation of the structure factor by one of three techniques: isomorphic heavy-atom replacement,[1,2] anomalous scattering,[3] and resonant Mössbauer scattering.[4] This method does not depend upon the use of large single crystals, since in all three techniques the unit-cell scattering amplitude is changed from $A_h = A_h^0 = -r_0 \mid F_h \mid e^{i\phi_h}$, where $r_0 = e^2/mc^2$ and $F_h = \mid F_h \mid e^{i\phi_h}$ is the structure factor, to $A_h = A_h^0 + A_h^1$, where A_h^1 is the added amplitude due to the extra scattering (heavy-atom, anomalous dispersion scattering, $f' + if''$, or resonant nuclear scattering, for the three cases). Since the integrated reflected intensity is directly proportional to $\mid A_h \mid^2$ for small crystals (kinematical approximation), ϕ_h can be deduced from knowledge of A_h^1 and measurement of $\mid A_h^0 \mid^2$ and $\mid A_h^0 + A_h^1 \mid^2$.

Two other methods of phase determination have been proposed which depend upon the use of thick (relative to the extinction length) crystals. In the first method (Colella,[5] Post,[6] and others[7,8]), one positions the crystal at a three-beam point, where two Bragg reflections, $\vec{\mathrm{K}}_1$ and $\vec{\mathrm{K}}_2$, simultaneously occur with appreciable amplitude. Then if $\vec{\mathrm{k}}_0$ is the incident wave vector, reflected waves with $\vec{\mathrm{k}}_1 = \vec{\mathrm{k}}_0 + \vec{\mathrm{K}}_1$ and $\vec{\mathrm{k}}_2 = \vec{\mathrm{k}}_0 + \vec{\mathrm{K}}_2$ are simultaneously excited. For thick crystals, the reflected wave in channel $\vec{\mathrm{k}}_1$ arises not only from the direct scattering from $\vec{\mathrm{k}}_0$, amplitude $\sim A_{\vec{\mathrm{K}}}$, but also by indirect scattering via $\vec{\mathrm{k}}_2$, amplitude $\sim A_{\vec{\mathrm{K}}_2} A_{\vec{\mathrm{K}}_1 - \vec{\mathrm{K}}_2}$. In this case, as Post has demonstrated, the intensity of the reflected wave in channel $\vec{\mathrm{k}}_1$ (or $\vec{\mathrm{k}}_2$) for $\vec{\mathrm{k}}_0$ in the vicinity of the three-beam point exhibits an intensity variation with $\vec{\mathrm{k}}_0$ which depends on the phase $(\phi_{\vec{\mathrm{K}}_1} - \phi_{\vec{\mathrm{K}}_2} - \phi_{\vec{\mathrm{K}}_1 - \vec{\mathrm{K}}_2})$. Measurements on a series of three-beam points determined by the pairs of reciprocal-lattice vectors $\vec{\mathrm{K}}_i, \vec{\mathrm{K}}_j$ can then be used to determine the phases.

Cowley[9] has pointed out the possibility of using Kossel lines[10–12] to obtain structure information. In a previous paper[13] two of us showed that, if the emitting atoms are near the crystal surface, the Kossel-line intensity profiles depend in a simple way upon the phase of the structure factor. A source of spherical waves at a position $\vec{\mathrm{R}}_i$ in a crystal emits a wave with a wave vector $\vec{\mathrm{k}}_1$ which is Bragg-reflected by the crystal into $\vec{\mathrm{k}} = \vec{\mathrm{k}}_1 + \vec{\mathrm{K}}_h$ with amplitude $\sim e^{-i\vec{\mathrm{k}}_1 \cdot \vec{\mathrm{R}}_i} \mathscr{R}_h(\vec{\mathrm{k}})$, where $\mathscr{R}_h(\vec{\mathrm{k}}) = e^{i\phi_h} \mathscr{D}(\Delta\theta / W_h)$. Here, ϕ_h is the phase of the structure factor, $\Delta\theta$ is the deviation from the dynamical Bragg angle, and W_h is the half-width of the total reflection region. $\mathscr{D}(\Delta\theta/W_h)$ is the usual Darwin reflection amplitude. This wave interferes with that emitted directly in the direction $\hat{k}$, which has an amplitude $\sim e^{-i\vec{\mathrm{k}} \cdot \vec{\mathrm{R}}_i}$, as shown schematically in Fig. 1. Thus the total amplitude of the wave traveling in the $\hat{k}$ direction is

$$\sim e^{-i\vec{\mathrm{k}} \cdot \vec{\mathrm{R}}_i} + e^{i\phi_h} e^{-i\vec{\mathrm{k}}_1 \cdot \vec{\mathrm{R}}_i} \mathscr{D}(\Delta\theta / W_h) .$$

The cross term in the resulting intensity depends upon the phase of the structure factor, allowing ϕ_h to be determined. Stephan *et al.*,[14] independently of us, also pointed out that Kossel-cone analysis could serve to determine the phases.

The simplest arrangement to use for determining the phases by this method is to have the sources confined near the crystal surface and to measure the Bragg-case Kossel lines resulting from reflected waves emerging through that surface. If the crystal is thick (relative to the Darwin extinction depth), and the sources are distributed near the surface, well within the extinction depth, the effect of scattering by the crystal layers between the sources and the surface will be quite small, and the data analysis to

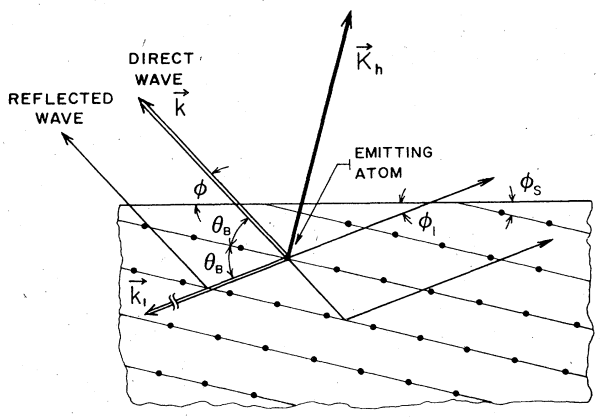

FIG. 1. Schematic of Bragg-case Kossel emission. The directly emitted waves are indicated by the double lines $\vec{k}$ and $\vec{k}_1$. The scattered waves are indicated by the single lines. θ_B is the Bragg angle, and ϕ_s is the angle between the scattering planes and the crystal surface, while ϕ and ϕ_1 are the angles between the crystal surface and the $\vec{k}$ and $\vec{k}_1$ directions, respectively.

determine the phases is greatly facilitated.

The advent of intense, tunable synchrotron x-ray sources should allow one to produce such a distribution of atomic sources near the surface in sufficient numbers to make this scheme practicable, as we discuss below. The use of this technique in phase-angle determination for centrosymmetric crystals is almost trivial, but it is also applicable to noncentrosymmetric crystals.

The paper of ours in which we originally noted the phase dependence at Kossel-line profiles[13] simply discussed the theoretical basis for this effect, but contained no analysis of its feasibility as an experimental technique. Experiments involving the measurement of Kossel lines have traditionally been regarded as very difficult to perform, due to the extremely narrow angular width of the line profiles. In this paper we show that such an experiment, while perhaps difficult, is quite feasible, despite "smearing" of the line profiles due to angular resolution and the inherent linewidth of the emitted x rays. In view of the present interest in solutions to the phase problem and the emerging importance of synchrotron radiation, we feel that such an experiment would be well worthwhile, and it is our hope that the present paper will stimulate interest in such an experimental program.

II. KOSSEL-LINE PROFILES IN THE BRAGG CASE

Kossel lines occur when atoms within a crystal emit x rays. Associated with this emission is both a direct outgoing spherical wave and scatterings of this wave corresponding to the various available Bragg reflections within the crystal. Near a Bragg angle the interference between the direct and scattered waves gives rise to a "light-dark" structure which depends on the phase angle of that reflection's structure factor.

The Laue-Bragg condition is satisfied for any value of the azimuthal angle about the reciprocal-lattice vector of the reflection, resulting in an interference cone whose apex angle is $\pi-2\theta_B$, where θ_B is the glancing angle of the reflection relative to the scattering planes (see Fig. 1).

The pure Bragg, or reflection, case occurs when the geometry is such that the entire cone for a particular reflection lies on one side of the crystal surface, as in Fig. 2(a). If a part of the cone dips below the crystal surface, as in Fig. 2(b), that part and a corresponding part on the opposite side of the cone correspond to the Laue, or transmission, case. The remainder of the cone is the Bragg case. The Bragg case is somewhat easier to analyze than the Laue case and we will restrict our attention to it in this paper.

Let us consider the simplest situation, consisting of an atom located at $\vec{R}_i$ on the surface of a crystal which emits a spherical outgoing wave of amplitude

$$\mathscr{A}(\vec{r})=\frac{e^{ik|\vec{r}-\vec{R}_i|}}{|\vec{r}-\vec{R}_i|}\,. \tag{1}$$

For the moment we will neglect the effects of polarization.

We take the surface at $z=0$ with the crystal filling the region $z<0$. If $k|\vec{r}-\vec{R}_i|\gg 1$, then, for $z<0$,[15]

$$\mathscr{A}_-(\vec{r})\approx\frac{ik}{2\pi}\int_< e^{i\vec{k}\cdot(\vec{r}-\vec{R}_i)}d\Omega_k\,, \tag{2}$$

where $\int_< d\Omega_k$ denotes integration over the lower hemi-

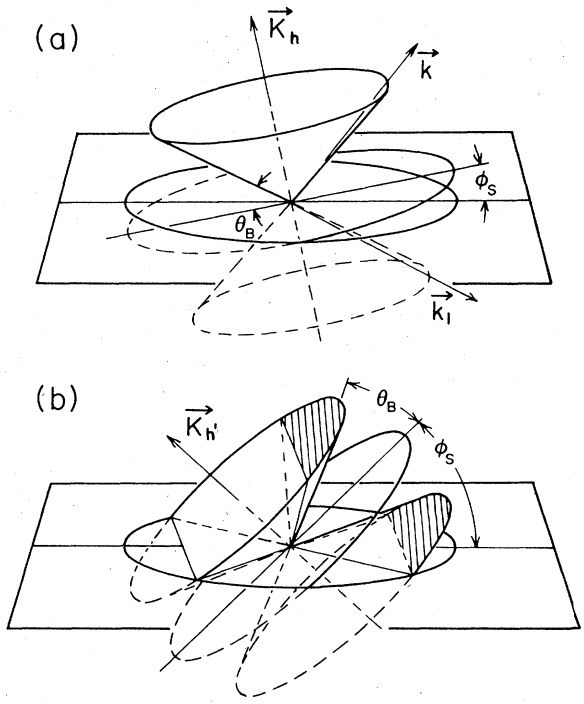

FIG. 2. Kossel-cone geometries. The pure Bragg case, panel (a), occurs when $\theta_B>\phi_s$. The entire cone then corresponds to reflection and lies above the crystal surface. The composite case, panel (b), $\theta_B<\phi_s$, contains both a Bragg (reflection) part and a Laue (transmission) part. The Laue part is shaded.

sphere ($k_z<0$). Equation (2) expresses the spherical wave [Eq. (1)] for $z<0$ as a sum of plane waves incident upon the crystal from above. These plane waves may then be treated using the Darwin multiple-scattering theory.[16] Most of the rays $\hat{k}$ penetrate into the crystal and are either absorbed or scattered incoherently. The rays, $\hat{k}_1$, however, which satisfy the Bragg condition for some set of Bragg planes within the crystal (reciprocal-lattice vector $\vec{K}_h$), will be partially reflected and re-emerge from the top face of the crystal. These reflected waves will form a cone about $\vec{K}_h$ which makes the Bragg angle with the set of reflecting planes, as shown in Fig. 1.

Only about half of the radiation is initially emitted into the lower hemisphere and only a small portion of that will be reflected (that emitted into the narrow Darwin width of the various Bragg reflections). The other half of the radiation will be emitted into the upper hemisphere, with amplitude ($k\,|\,\vec{r}-\vec{R}_i\,|\gg 1$)

$$\mathscr{A}_+(\vec{r})\approx\frac{ik}{2\pi}\int_> e^{i\vec{k}\cdot(\vec{r}-\vec{R}_i)}d\Omega_k\ , \tag{3}$$

where now the integration is over the upper hemisphere, $k_z>0$. By itself, $\mathscr{A}_+$ would give a uniform intensity distribution over the upper hemisphere. In certain directions, however, there will be an additional contribution due to the waves which have been Bragg-reflected into the $z>0$ region. In these directions, interference will occur and the resulting intensity will depend upon the relative phases of the directly emitted and the reflected waves.

Now let $\vec{k}$ ($k_z>0$) lie very near a Bragg angle to a set of crystal planes. There is a unique $\vec{k}_1$ ($k_{1z}<0$) which is reflected into $\vec{k}$ by this set of planes. The Darwin expression for the amplitude of the reflected wave is then[17,18]

$$\begin{aligned}\mathscr{A}_R(\vec{r})&\approx\frac{ik}{2\pi}\int_> e^{i(\vec{k}\cdot\vec{r}-\vec{k}_1\cdot\vec{R}_i)}e^{i\phi_h}\mathscr{D}(\Delta\theta/W_h)d\Omega_k\\&\approx\frac{ik}{2\pi}\int_> e^{i(\vec{k}\cdot\vec{r}-\vec{k}_1\cdot\vec{R}_i)}e^{i\phi_h}\left\{\frac{\Delta\theta}{W_h}+\left[\left[\frac{\Delta\theta}{W_h}\right]^2-1\right]^{1/2}\right\}^{-1}\left[\frac{\sin\phi}{\sin\phi_1}\right]^{1/2}d\Omega_k\ ,\end{aligned} \tag{4}$$

where ϕ_h is the phase of the unit-cell structure factor

$$|F_h|\,e^{i\phi_h}=\int_{\text{unit cell}} e^{-i\vec{K}_h\cdot\vec{r}'}\rho(\vec{r}')d\vec{r}'\ , \tag{5}$$

$\rho(\vec{r}')$ being the electron density. ϕ and ϕ_1 are the angles that $\vec{k}$ and $\vec{k}_1$ make with the surface of the crystal, respectively, $\Delta\theta$ is the deviation from the dynamical Bragg angle θ_B, taken in the same sense as θ_B. The sign of the radical $[(\Delta\theta/W_h)^2-1]^{1/2}$ in Eq. (4) is the same as that of $\Delta\theta$ when $|\Delta\theta/W_h|>1$, and is positive imaginary when $|\Delta\theta/W_h|<1$. W_h is the half-width of the Darwin total reflection region, given by

$$W_h=C\frac{ne^2\lambda^2}{\pi mc^2}\frac{|F_h|}{\sin(2\theta_B)}\left[\frac{\sin\phi_1}{\sin\phi}\right]^{1/2}. \tag{6}$$

Here, n is the number density of unit cells, λ is the wavelength of the emitted radiation, and C is a polarization factor equal to 1 for σ polarization ($\vec{E}$ perpendicular to the scattering plane) and $\cos(2\theta_B)$ for π polarization ($\vec{E}$ parallel to the scattering plane).

Adding the directly emitted wave $\mathscr{A}_+(\vec{r})$, Eq. (3), to the reflected wave $\mathscr{A}_R(\vec{r})$, Eq. (4), we have, for the total wave amplitude (for $z>0$, $k\,|\,\vec{r}-\vec{R}_i\,|\gg 1$, and $\hat{k}$ near the Bragg angle for the reflection $\vec{K}_h$),

$$\begin{aligned}\mathscr{A}_{\text{tot}}(\vec{r})&\simeq\frac{ik}{2\pi}\int_> e^{i\vec{k}\cdot\vec{r}}\left[e^{-i\vec{k}\cdot\vec{R}_i}+e^{-i\vec{k}_1\cdot\vec{R}_i}e^{i\phi_h}\mathscr{D}\left[\frac{\Delta\theta}{W_h}\right]\right]d\Omega_k\\&\simeq\frac{ik}{2\pi}\int_> e^{i\vec{k}\cdot(\vec{r}-\vec{R}_i)}\left[1+e^{i\vec{K}_h\cdot\vec{R}_i}e^{i\phi_h}\mathscr{D}\left[\frac{\Delta\theta}{W_h}\right]\right]d\Omega_k\\&\simeq\frac{e^{ik|\vec{r}-\vec{R}_i}}{|\vec{r}-\vec{R}_i|}\left[1+e^{i\vec{K}_h\cdot\vec{R}_i}e^{i\phi_h}\mathscr{D}\left[\frac{\Delta\theta}{W_h}\right]\right].\end{aligned} \tag{7}$$

In the second line of Eq. (7), we used the Bragg condition $\vec{k}_1\simeq\vec{k}-\vec{K}_h$, and in the third line we supposed that $|\,\vec{r}-\vec{R}_i\,|$ was sufficiently large (Fraunhofer diffraction region) that we could replace $\mathscr{D}(\Delta\theta/W_h)=\mathscr{D}(\vec{k})$ by $\mathscr{D}[k(\vec{r}-\vec{R}_i)/|\,\vec{r}-\vec{R}_i\,|\,]$ in the integral over solid angles, and we then evaluated the integral by the method of stationary phase. Thus, the variation in intensity across the Kossel cone, relative to the background intensity well

away from the cone, is given by

$$R(\Delta\theta)=\left|1+e^{i\vec{K}_h\cdot\vec{R}_i}e^{i\phi_h}\mathscr{D}\left(\frac{\Delta\theta}{W_h}\right)\right|^2 . \tag{8}$$

Now, $\exp(i\vec{K}_h\cdot\vec{R}_i)$ is unchanged by the substitution $\vec{R}_i\rightarrow\vec{R}_i+\vec{l}$, where $\vec{l}$ is any Bravais-lattice vector. Thus, $R(\Delta\theta)$ depends only upon the location of $\vec{R}_i$ within the unit cell, i.e., all sources whose locations differ only by a Bravais-lattice vector will give the same intensity. If there is only one source per unit cell, we may take $\vec{R}_i$ as the origin in Eq. (5). Since the phase of $\mathscr{D}(\Delta\theta/W_h)$ increases by π as $\Delta\theta$ sweeps through the Kossel cone, ϕ_h is uniquely determined by $R(\Delta\theta)$, Eq. (8), and ϕ_h can thus be found by accurately measuring the intensity profile of the Kossel cone.

As is necessarily the case, if one wants to determine the *phase* of a scattered wave, one must "beat it" with a coherent reference wave. In our case the coherent reference wave is that emitted directly into the $\hat{k}$ direction.

The internal source problem has usually been solved by means of the reciprocity theorem of Lorentz and Laue.[11] Equation (8) for $R(\Delta\theta)$ may also be obtained using that method. The "direct approach" used here has proved valuable, however, since it makes it obvious from holographic considerations that ϕ_h may be determined by observations of Kossel-cone intensities.

If the atom is not on the surface, but below it by some distance d, we must multiply Eq. (8) by an exponential damping factor, $e^{-\zeta d}$, where ζ gives the correction for scattering due to the crystal layers between the emitting atom and the crystal surface (primary extinction), as well as for absorption.[17] Because of the exponential damping it will be desirable to confine the emitting atoms to a layer well within one extinction depth of the surface. In this case we may neglect absorption effects, and ζ is then given by

$$\zeta=\frac{2Cn\lambda e^2}{mc^2}|F_h|(\sin\phi\sin\phi_1)^{-1/2}\left[1-\left(\frac{\Delta\theta}{W_h}\right)^2\right]^{1/2} . \tag{9}$$

If polarization effects are taken into account, Eq. (8) is further modified in a way which depends upon the multipole of the emitted radiation. For the E1 (electric dipole) radiation of interest here, the final expression for $R(\Delta\theta)$ is as follows:

$$\begin{aligned}R(\Delta\theta)&=\left\{1+C\left[e^{i\phi_h}\mathscr{D}\left(\frac{\Delta\theta}{W_h}\right)+\text{c.c.}\right]+\left|\mathscr{D}\left(\frac{\Delta\theta}{W_h}\right)\right|^2\right\}e^{-\zeta d}\\&=\left[1+C\left(\frac{\sin\phi}{\sin\phi_1}\right)^{1/2}\left\{e^{i\phi_h}\left\{\frac{\Delta\theta}{W_h}+\left[\left(\frac{\Delta\theta}{W_h}\right)^2-1\right]^{1/2}\right\}^{-1}+\text{c.c.}\right\}+\frac{\sin\phi}{\sin\phi_1}\left|\frac{\Delta\theta}{W_h}+\left[\left(\frac{\Delta\theta}{W_h}\right)^2-1\right]^{1/2}\right|^{-2}\right]e^{-\zeta d} .\end{aligned} \tag{10}$$

For a detailed, technical derivation of Eq. (10), as well as similar expressions for radiation of other multipoles, we refer the interested reader to Ref. 13.

For symmetric Bragg cones ($\phi_s=0$ in Fig. 1), $\phi=\phi_1$ and $\Delta\theta=\Delta\phi$, where $\Delta\phi$ is the change in the glancing angle relative to the crystal surface. In this case there is no variation in the line profile with azimuthal angle. For the nonsymmetric Bragg cones ($\phi_s\neq0$), however, $\Delta\theta\neq\Delta\phi$, in general, and there will be a variation in the line profile around the cone, as expressed in Eq. (10).

Both polarizations, σ and π, occur with equal probability and, due to the factor of C in W_h [Eq. (6)], they have different linewidths. The line profile is a result of the superposition of these two polarizations. However, since W_h is quite small ($\sim10^{-5}$ rad) and the energy width of the emitted x ray, $\Delta k/k$, is of the order of 10^{-4}, this structure will not be resolved.

If we integrate across the line profile, we obtain the excess integrated intensity $S_{2\Delta}$, where 2Δ is the range of integration. $S_{2\Delta}$ is given by

$$\begin{aligned}S_{2\Delta}&=\frac{\sum_\alpha\int_{-\Delta}^{\Delta}[I_\alpha(\Delta\theta)-I_{\alpha B}]d(\Delta\theta)}{\sum_\alpha\int_{-\Delta}^{\Delta}I_{\alpha B}d(\Delta\theta)}\\&=(4\Delta)^{-1}\sum_\alpha\int_{-\Delta}^{\Delta}[R_\alpha(\Delta\theta)-1]d(\Delta\theta) ,\end{aligned} \tag{11}$$

where α refers to the two polarizations, σ and π.[17]

If the effects of extinction and the finite angular resolution of the apparatus are neglected, then

$$S_{2\Delta}=\frac{W_{h\sigma}}{2\Delta}\frac{\sin\phi}{\sin\phi_1}\left[\tfrac{4}{3}[1+\cos(2\theta_B)]+\pi\cos(2\theta_B)\left(\frac{\sin\phi}{\sin\phi_1}\right)^{1/2}\sin\phi_h\right],\quad \Delta\gg W_{h\sigma} . \tag{12}$$

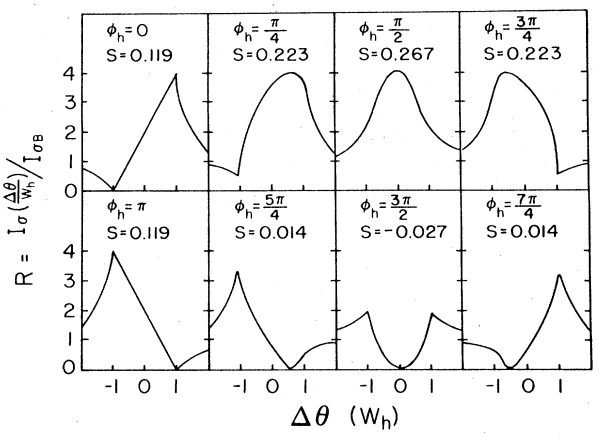

FIG. 3. Kossel-line rocking curves for the σ-polarization Bragg case for different values of the phase angle ϕ_h of the structure factor. $W_{h\sigma}$ is the half-width of the total reflection region, while $\Delta\theta$ is the angle of emission relative to the dynamical Bragg angle. The values of the excess integrated intensity $S_{2\Delta}$ (shown as S in this figure) are for the Ga[333] line of GaAs, σ polarization only, and correspond to $\Delta = 10W_{h\sigma}$. Note that the pairs $(0,\pi)$, $(\pi/4, 3\pi/4)$, and $(5\pi/4, 7\pi/4)$ each give the same excess integrated intensity but have line profiles of opposite polarity.

In practice, if the range of emitter depths and the source size are sufficiently limited, these two effects will be very small, and $S_{2\Delta}$ will still exhibit the sinusoidal dependence on ϕ_h, essentially as given by Eq. (12). Note, also, that in inverting the above equation, the phase angle ϕ_h is a two-valued function of $S_{2\Delta}$. The two phase angles producing the same integrated intensity will, however, have line profiles of opposite polarity (light-dark as opposed to dark-light), as follows from Eq. (10) and is exhibited in Fig. 3, *and a qualitative examination of this polarity will remove this degeneracy. For a centrosymmetric crystal, the values of ϕ_h are restricted to 0 or π. In this case an examination of this polarity alone suffices to determine ϕ_h.*

III. PROPOSED EXPERIMENT

For ease of analysis it will be important to have the emitting atoms confined to a small region near the surface of the crystal, whose depth is not more than some fraction of the shortest extinction depth, $[\zeta(\Delta\theta=0)]^{-1}$, of any cone being observed. In addition, it will be necessary to limit the lateral extent of the source region, in order to ensure sufficient angular resolution to observe the polarity of the line profiles. Below a certain limit, however, little is gained by further decreasing the source size since the energy width of the emitted x ray ($\Delta k/k \sim 10^{-4}$) becomes the dominant resolution-determining effect.

A focused beam of synchrotron radiation provides a good method for generating such a source. A monochromatic slice of the beam may be selected so as to lie directly on the K edge of a particular species of atom in the crystal, assuring that a large proportion of the excited atoms will be of that species. Such a focused beam is very intense and will generate a large number of excitations per second within the crystal. Sparks[19] has shown that with currently available synchrotron sources and focusing arrangements it is possible to obtain a 10-keV beam of 1.1 eV width with a flux density of 7.4×10^8 photons $s^{-1}\mu m^{-2}$ using asymmetrically cut Ge(111) crystals, doubly curved to a demagnification factor of 10.[20] Even higher demagnification factors might be possible,[21] and, in addition, the use of wigglers should allow even higher flux densities.[19]

There are several geometries which might be used to generate a source of emitting atoms confined to the surface of the crystal. In an idealized arrangement, if the desired source depth is d, a nib might be etched into a suitable area of the crystal surface of height somewhat greater than d, as shown in Fig. 4(a). This nib might then be inserted into the focused spot of the synchrotron beam to the desired depth. While the physical extent of the beam spot would not have a sharp cutoff and the sources

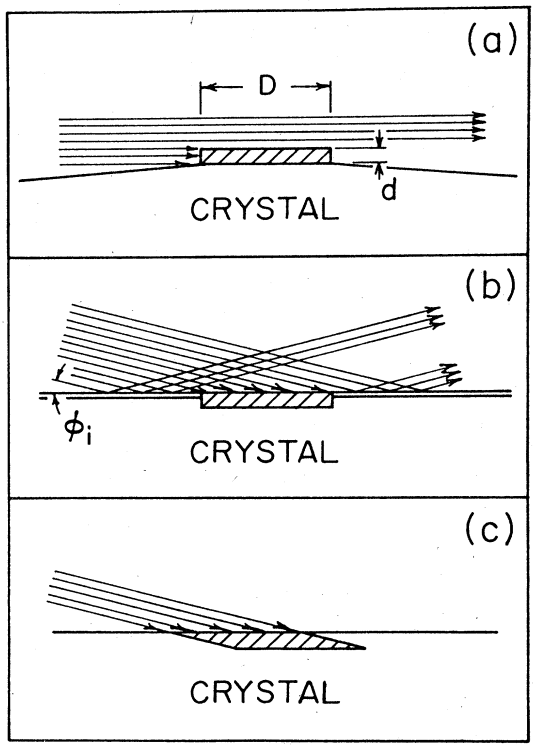

FIG. 4. Schematic diagram of three possible source geometries, not to scale. The shaded area represents the resulting source region in each case. In (a) the focused synchrotron beam strikes a projecting nib from the side. Those photons which do not excite atoms within the nib pass through and out the other side, not deeper into the crystal. In (b) the beam strikes the crystal surface at an angle ϕ_i above the critical reflection angle of the crystal itself, but below that of a reflective coating which surrounds the nib. Thus those photons not striking the nib would be reflected away. In (c) the beam is focused and collimated to a size sufficiently small to be used directly, the area of the crystal surface illuminated being the size of the desired source region. The depth of the distribution of emitting atoms is determined by the glancing angle of the beam with the crystal surface.

would not be uniformly distributed with depth, a large majority of them would occur very near the surface. As long as this is true, the exact distribution of the emitting atoms with depth will not be critical, since the effects of extinction will be small in any case.

A second possible geometry relies upon grazing incidence to limit the source size and depth. The surface around the above-mentioned nib could be coated with some higher-Z material, as in Fig. 4(b). If the focused synchrotron beam were then incident at an angle above the critical angle of the crystal, but below that of the surrounding coating, the radiation striking the coating would be reflected away. That striking the nib, on the other hand, would penetrate to a depth of ϕ_i times the off-Bragg absorption length. As long as ϕ_i is kept sufficiently small, the depth over which the emitting atoms will be distributed will be adequately controlled. The reflective coating would not interfere with the observation of the Kossel lines since it will be essentially transparent to radiation striking it at angles greater than its critical reflection angle ($\sim 10^{-3}$ rad).

The simplest possible geometry, that shown in Fig. 4(c), would require collimating and focusing the synchrotron beam down to a very small height, so that when striking the crystal at a small angle, the length of the area illuminated on the surface is equal to that of the desired source region. The width of the focused synchrotron beam should equal the width of the desired source region. As an example, if the beam could be reduced to 1 μm in height and if it struck the crystal at an angle of 10^{-2} rad, the illuminated area of the surface would then be only 100 μm long. If the off-Bragg absorption length were about 10 μm (as in the case of GaAs, considered below), the source region so generated would be about 1000 Å deep.

With any of these source geometries, the actual distribution of emitting atoms with depth will depend upon the spatial distribution of the focus spot of the synchrotron beam. The line profiles shown in this paper were calculated assuming an idealized source region 30 μm in diameter and 0.1 μm deep.

Since many Bragg reflections will be available within the crystal, many Kossel lines will be produced simultaneously. A principal advantage of this method of phase determination lies in the fact that, utilizing film techniques, it should be possible to detect large regions of the circumference of each of the Kossel lines in a single run. Thus many phase angles can be measured simultaneously.

For the present analysis, we assumed a hemispherical chamber at 0.5 m radius, as shown in Fig. 5, with the crystal fixed at the center. Strips of film would then be placed along the inner surface of the hemisphere at the positions where the Kossel lines would be expected to appear. It will be necessary to evacuate the chamber, since appreciable absorption of 10-keV x rays would occur in air.[22]

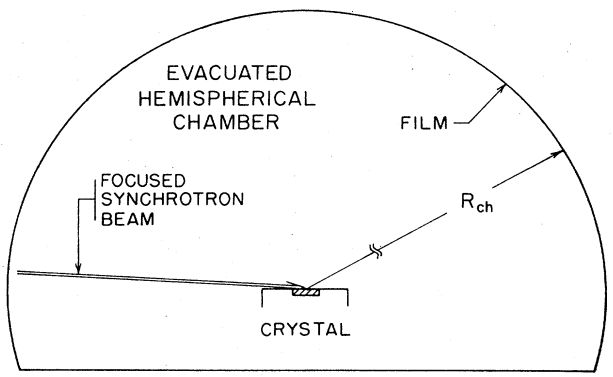

FIG. 5. Schematic diagram of the proposed experimental apparatus, not to scale. R_{ch} is the radius of the evacuated hemispherical chamber.

IV. EXAMPLE—GaAs

As a practical example, consider exciting the Ga atoms in a GaAs crystal cut along a (111) face. This crystal was chosen as an illustration for three reasons. First, it is a simple example of a noncentrosymmetric crystal (zinc-blende structure). Second, the $K\alpha$ emission of Ga, $\lambda = 1.34$ Å, is sufficiently short in wavelength to provide good resolution of the structure of the unit cell. Third, the other constituent of the unit cell, namely the As atom, is sufficiently high Z to provide a wide variation in the phase angles of the structure factors for the various reflections.

The shortest extinction depth for this crystal in this geometry is that of the [111] reflection, 3300 Å at the center of the total reflection region for the σ-polarization line. The linear absorption depth at this energy is 37 μm, 2 orders of magnitude larger. If the depth of the emitting region is limited to 1000 Å, the effect of extinction on the [111]-line profile will be very small and nearly negligible for the other lines produced. Absorption will be negligible in all cases. As previously mentioned, the calculations in this paper were carried out assuming a 30-μm-diam source region containing excited atoms uniformly distributed to a depth of 1000 Å.

At the Ga K edge (10.38 keV) the photoelectric cross section for Ga is 2.5×10^{-4} Å^2, while that of As is 5.0×10^{-5} Å^2.[23] The Compton cross section is negligible in each case. Thus 83% of the excitations occurring within the crystal will be Ga, the 17% As decays contributing to a uniform background in the neighborhood of the Ga-produced Kossel lines. Of the Ga excitations, approximately 58% will decay through $K\alpha_1$ emission ($\lambda = 1.340$ Å), 29% through $K\alpha_2$ emission ($\lambda = 1.344$ Å), and 12% through $K\beta_1$ emission ($\lambda = 1.209$ Å). With an incident flux density of 7.4×10^8 photons s^{-1} μm^{-2} and a cross-sectional area of 30×0.1 μm^2 of the source region presented to the beam, 2×10^9 photons will strike the source every second. As an example, for the geometry shown in Fig. 4(a), this would result in a total flux at 1.5×10^9 decays s^{-1}, of which 1.2×10^9 would be from Ga. With a 0.5-m source-to-film distance, this implies a background flux density of 1.4×10^{-3} photons s^{-1} μm^{-2} on the film. A typical fine-grain x-ray film (Morimoto and Uyeda,[24] film No. 7) requires 0.33 photons μm^{-2} at this energy to achieve an optical density of 0.25. This implies a run time of the order of 220 s.

The resolution of such a system should be sufficient to

distinguish easily between the $K\alpha_1$ and $K\alpha_2$ peaks in all lines observed. Calculated line profiles for the worst case, that of the [111] line, are shown in Fig. 6, the two peaks being separated by 0.3 mm on the film. In all other lines, the separation will be larger due to the larger values of θ_B, so that for the [333] line, for example, the two peaks will be separated by 1.2 mm. The $K\alpha_1$ and $K\alpha_2$ peaks will be virtually identical except for their intensity, since the difference in their wavelengths is only 0.3%.

In Fig. 7 we show the calculated line profiles for either emission channel, $K\alpha_1$ or $K\alpha_2$, normalized to that channel's background intensity, for the [111] and [333] Kossel cones. Also shown are the final profiles, obtained from the calculated true profiles by successive convolution of a Gaussian angular resolution function of width

$$\sigma=(D\sin\theta+d\cos\theta)/R_{\rm ch}+\frac{\Delta k}{k}\tan\theta\ ,$$

in rad, and a square distribution corresponding to a microdensitometer slit 0.03 mm wide. The first term in σ gives the angle subtended by the source (diameter D and depth d) at the film surface, $R_{\rm ch}$ being the radius of the hemispherical chamber, while the second term gives the broadening due to the energy width of the emitted x ray. Since for this case, $\Delta k/k=1.23\times10^{-4}$, the second term is by far the largest and is the main reason why little resolution is gained by increasing the crystal-to-film distance. It can be seen in Fig. 7(b) that the fine structure in the line profiles due to the two polarizations present is lost after convolution and will not be observed. The polarity of the line profiles will still be distinguishable, however.

The principal measurement which should be used to obtain the phase angle of the structure factor will be the excess integrated intensity $S_{2\Delta}$ [Eq. (11)]. If integration limits (2Δ) are chosen to be 10 times the full width of the total reflection region of the σ-polarization line in each case, the excess integrated intensity in the [111] cone will be 0.0128, while that in the [333] cone will be 0.1365.

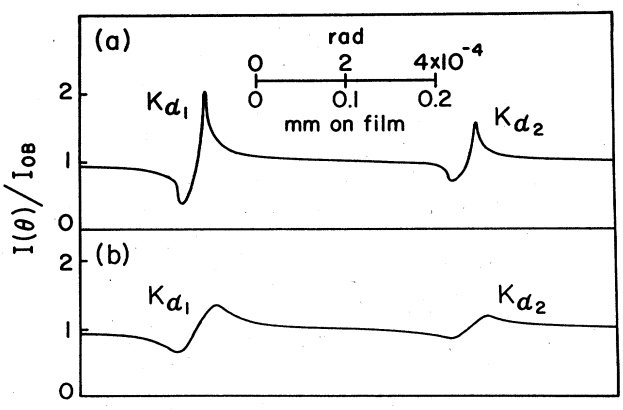

FIG. 6. Calculated Kossel-line rocking curves for the Ga[111] line of GaAs, showing the $K\alpha_1$ and $K\alpha_2$ peaks. The two peaks are separated by 0.3 mm on the film. The convoluted plot, panel (b), is that which would be traced by the microdensitometer directly from the film, neglecting statistical variation due to film granularity.

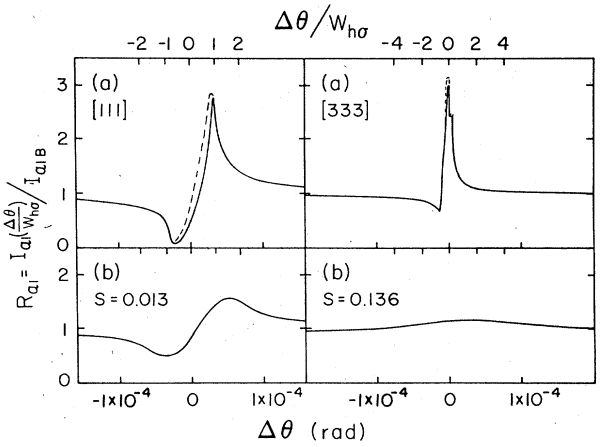

FIG. 7. Calculated Kossel-line rocking curves for the Ga[111] and Ga[333] lines of GaAs. Plot (a) is before convolution and plot (b) is after. Dotted lines show the line profiles neglecting extinction. The structure visible in the unconvoluted [333] line is due to the two polarizations present.

These values were calculated from the line profiles after convolution and represent phase angles of either $-46.5°$ or $-135°$ in the [111] case, and either $+46.2°$ or $+134°$ in the [333] case. An examination of the polarity of the line profile will in each case rule out the latter value. In this way the phase angle may be fully determined by the measurement of Kossel-line profiles.

If the crystal had been centrosymmetric with the emitting atom lying at the center of symmetry, the only possible phase angles would be 0 or π. Both these phase angles would give rise to the same value of $S_{2\Delta}$. A qualitative examination of the line profiles, however, is all that would be required to determine the phase angle, since, again, the two possibilities will give rise to line profiles of opposite polarity.

V. UNCERTAINTY AND SOURCES OF ERROR

The quality of this measurement should be principally affected by three sources: resolution effects, statistical errors, and systematic errors. The resolution of the system will be determined chiefly by the width, $\Delta k/k$, of the emitted x ray, and secondarily by the size of the emitting region and the width of the microdensitometer slit. The effect of this limited angular resolution will be to smear out the details of the line profiles, but it should not seriously effect the integrated intensity, as long as the integration limits are sufficiently large.

The statistical errors will be principally determined by the size of the microdensitometer slit and by the granularity of the film. The width of the microdensitometer slit used to convolute the line profiles was chosen for this analysis at 0.03 mm as being as small as practical. Beu[25] reports that a slit of (4.0×0.05) mm^2 area is about the practical limit for use with fine-grain x-ray film. Owing to the large crystal-to-film distance proposed for this experiment, however, the Kossel lines on the film will show

very little curvature and the slit width may be increased to 1 cm or even larger without seriously affecting the results. Alternately, the slit may be curved to match the curvature of the Kossel line being measured, allowing an even greater increase in length.

A typical fine-grain x-ray film has a Selwyn granularity of approximately 2.2 μm.[24] With a scanning area of (10.0×0.03) mm^2, one standard deviation of any measurement of optical density on such a film will be 0.0028, or 1.1% of an optical density of 0.25. There will be, however, an enormous amount of data which may be analyzed. With a 0.5-m crystal-to-film distance, the circumference of the [111] line will be 3.85 m. If the line profile were to be measured at some 280 points along this line, the fluctuation due to granularity could be reduced by a factor of $\sqrt{280}$, i.e., to 0.07% of background, essentially negligible.

Symmetric Bragg lines were chosen for this analysis for the sake of simplicity, since for these lines the line profile is independent of azimuthal angle. For nonsymmetric Bragg lines, in which the scattering planes are not parallel to the surface, the line profile does depend on this angle. The above comments remain valid, nevertheless, as long as this variation is taken into account and corrected for.

The other major contributions to the statistical uncertainty, variations in film sensitivity and random misalignments of the integration limits with the center of the total reflection region, should make negligible contributions for the same reason. Averaging over the large amounts of data available for each line will essentially eliminate this contribution to the uncertainty.

The major contribution to the uncertainty in the measurement of the phase angle will be a systematic one. As can be seen in Fig. 7, the line profile remains above background on one side of the peak, but dips below on the other. In fact, for large values of $\Delta\theta/W_h$, the interference term goes like $(\Delta\theta/W_h)^{-1}$, and the integral of either half of the line profile diverges logarithmically. When the limits of integration are exactly centered over the total reflection region, however, the two sides of the interference term should cancel out, and this term will not contribute to the excess integrated intensity for $|\Delta\theta/W_h|>1$. If the limits of integration are not centered correctly this will no longer be true, and a systematic misalignment of this kind will result in an erroneous value of the integrated intensity and thus an incorrect phase angle.

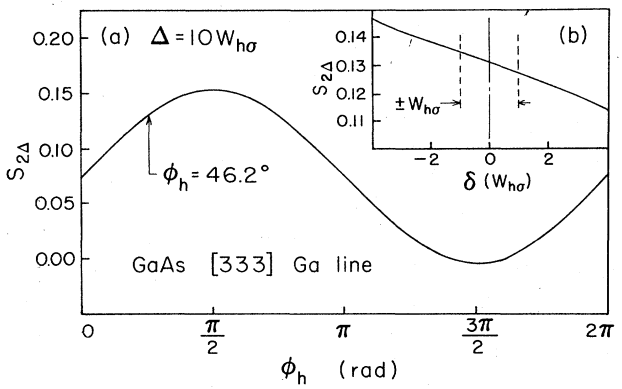

FIG. 8. Variation of the excess integrated intensity $S_{2\Delta}$ of the Ga[333] line of GaAs as a function of ϕ_h, the phase of the structure factor, panel (a). Also shown is the variation of $S_{2\Delta}$ with misalignment of the integration limits relative to the center of the total reflection region, panel (b). The dotted lines indicate misalignments of $\pm W_{h\sigma}$, the half-width of the σ-polarization total reflection zone. Values of $S_{2\Delta}$ were calculated assuming $\Delta=10W_{h\sigma}$.

As an order-of-magnitude estimate of the extent of this effect, consider the following. In Fig. 8 we show both the calculated variation of $S_{2\Delta}$ with phase angle and the calculated variation of $S_{2\Delta}$ with misalignment of the integration limits for the true phase angle of 46.2° for the [333] Kossel line. A misalignment of one times the half-width of the total reflection region to the right would result in a phase angle of 50.3°; one to the left, 42.2°. It should be possible to determine the center of the total reflection region to at least this accuracy, and thus the phase angle of this Kossel line within an uncertainty of ±4°. The accuracy will be somewhat less for phase angles in the neighborhood of $\pi/2$ or $3\pi/2$, where $\sin\phi_h$ is fairly flat. If the center of the total reflection region can be identified to a greater accuracy, the uncertainty in the measured phase angle will be correspondingly less.

VI. CONCLUSION

The technique described in this paper should be most applicable to the measurement of phase angles in crystals which have at least one high-Z constituent within the unit cell. The atom chosen as the emitter should have $Z>30$ in order to ensure a resolution of the order of 1 Å, and it should not occur more than a few times in each unit cell, preferably only once. If it occurs more than once the structure factor must be averaged over the various emitting sites, and some information will be lost.[13] For crystals in which there are no high-z atoms, it may be desirable to combine this technique with that of isomorphic heavy-atom replacement. The heavy atoms in the resulting crystal may then be used as the emitters to produce the Kossel-line patterns.

The use of this technique will also be contingent upon finding a sufficiently large region of single crystal so that nearly all the scattering will take place within a single mosaic block. This requirement, and their sensitivity to radiation damage, may limit the usefulness of Kossel-line analysis in the case of biological crystals, although this will depend upon the particular crystal under consideration. Once a suitable region of an appropriate crystal has been found, application of this technique should allow a large amount of information to be collected within a short period of time. If a number of such specimens were prepared, each cut along a different plane, the structure of the crystal might be characterized by only a small number of measurements, since each specimen will provide phase angles for several reflections.

The geometry proposed here is only one of many possible geometries which could be used, and it was chosen to

demonstrate the feasibility of such an experiment. We feel that when the criteria for applicability of this technique are met, the use of Kossel lines to measure the phase angles of structure factors should provide a useful alternative to other methods currently available.

ACKNOWLEDGMENTS

This work was supported by the National Science Foundation—Materials Science Program under Grant No. DMR-80-15706.

[1]D. M. Blow and F. H. C. Crick, Acta Crystallogr. **12**, 794 (1959).

[2]T. L. Blondell and L. N. Johnson, *Protein Crystallography* (Academic, New York, 1976).

[3]Goran Wendin, Phys. Scr. **21**, 535 (1980).

[4]E. Parak, R. L. Mössbauer, U. Biebl, H. Formanek, and W. Hoppe, Z. Phys. **244**, 456 (1971).

[5]R. Colella, Acta Crystallogr. Sect. A **30**, 413 (1974); Z. Naturforsch **37a**, 437 (1982).

[6]Ben Post, Phys. Rev. Lett. **39**, 760 (1977); **39**, 1108(E) (1977); Acta Crystallogr. Sect. A **35**, 17 (1979).

[7]Shih-Lin Chang, Appl. Phys. A **26**, 221 (1981); Phys. Rev. Lett. **48**, 163 (1982).

[8]Hellmut J. Juretschke, Phys. Lett. **92A**, 183 (1982).

[9]J. M. Cowley, Acta Crystallogr. **17**, 33 (1964).

[10]W. Kossel, V. Loeck, and H. Voges, Z. Phys. **94**, 139 (1935).

[11]M. von Laue, *Roentgenstrahl-interferenzen* (Akademische Verlagsgesellschaft, Frankfurt, West Germany, 1960).

[12]R. W. James, *The Optical Principles of the Diffraction of X-Rays* (Cornell University Press, Ithaca, N. Y., 1965).

[13]J. P. Hannon and G. T. Trammell, *Mössbauer Effect Methodology* (Plenum, New York, 1974), Vol. 9, pp. 181—190; Phys. Rev. B **9**, 2791 (1974); **9**, 2810 (1974).

[14]D. Stephan, W. Blau, H. J. Ullrich, and G. E. R. Schulze, Krist. Tech. **9**, 707 (1974); **11**, 475 (1976).

[15]J. P. Hannon, N. J. Carron, and G. T. Trammell, Phys. Rev. B **9**, 2791 (1974), especially Sec. IV.

[16]C. G. Darwin, Philos. Mag. **27**, 315 (1914); **27**, 675 (1914).

[17]J. P. Hannon, N. J. Carron, and G. T. Trammell, Phys. Rev. B **9**, 2810 (1974), especially Sec. III A.

[18]Note that the following changes in notation from that used in Ref. 9 have been made to agree with that commonly used for electronic scattering. Here, θ_B is the Bragg angle, rather than the scattering angle, and ϕ_h is the phase of the structure factor, rather than that of the unit-cell scattering amplitude.

[19]C. J. Sparks, Jr., *Synchrotron Radiation Research* (Plenum, New York, 1980), pp. 459—512.

[20]D. W. Berreman, J. Stamatoff, and S. J. Kennedy, Appl. Opt. **16**, 2081 (1977).

[21]W. J. Boettinger, H. E. Burdette, and Masao Kuriyama, Rev. Sci. Instrum. **50**, 26 (1979).

[22]George L. Clark, *Handbook of X-Rays* (McGraw-Hill, New York, 1967), Chap. 1, p. 21.

[23]*International Tables of X-Ray Crystallography* (Kynoch, Birmingham, 1968), Vol. III.

[24]Hidetake Morimoto and Ryozi Uyeda, Acta Crystallogr. **16**, 1107 (1963).

[25]Karl E. Beu, Rev. Sci. Instrum. **24**, 103 (1953).